Acoustic Scattering Problems with Convolution Quadrature and the Method of Fundamental Solutions

I. Labarca and R. Hiptmair

ACOUSTIC SCATTERING PROBLEMS WITH CONVOLUTION QUADRATURE AND THE METHOD OF FUNDAMENTAL SOLUTIONS*

IGNACIO LABARCA[†] AND RALF HIPTMAIR[‡]

Abstract. Time domain acoustic scattering problems in two dimensions are studied. The numerical scheme relies on the use of Convolution Quadrature (CQ) method to reduce the time domain problem to the solution of frequency domain Helmholtz equations with complex wavenumbers. These equations are solved with the method of fundamental solutions (MFS), which approximates the solution by a linear combination of fundamental solutions defined at source points inside (outside) the scatterer for exterior (interior) problems. Numerical results show that the coupling of both methods works efficiently and accurately for multistep and multistage based CQ.

Key words. acoustic wave scattering, convolution quadrature, method of fundamental solutions

1. Introduction. For several years now, since the seminal work of Ch. Lubich [17, 18], convolution quadrature (CQ) has attracted considerable attention as a method for simulating wave propagation in time domain, based on relationships obtained in the Laplace domain. This approach was successful in the wave propagation context, because it allows the use of frequency-domain Green's functions instead of their more complicated time-domain counterparts (see Eq.(1.2)).This makes possible the use of integral equation methods to solve the arising frequency-domain problems. Integral equation methods are also an option in time-domain, but they require difficult integration techniques in two dimensions, and dealing with distributional expressions in three dimensions [14]. Instead of resorting to integral equations, we follow a different and simpler approach. This is the method of fundamental solutions (MFS) [10, 4] which assumes that the solution of the Helmholtz equation can be represented by a linear combination of fundamental solutions with sources located at the interior of the scatterer. The advantage of the MFS for the CQ scheme also lies in the possibility of sparsification of the resulting matrix, due to the exponential decaying of fundamental solutions for modified Helmholtz equations [7]. It is also possible to use techniques developed for Boundary Element methods, which allow the use of directional $\mathcal{H}-$matrices for each of the Helmholtz problems [6]. Although a combination of MFS with Laplace transform techniques and the modified Helmholtz equation has been mentioned before [7, 16], as far as we know, there are no results for a successful implementation of MFS in combination with multistep and multistage methods in time domain, on which CQ is based.

The problem that we are interested in solving is the exterior (interior) acoustic scattering problem in the time-domain. Let $\Omega \subset \mathbb{R}^d$, $d = 2, 3$, be the bounded region of space occupied by the scatterer. By rescaling we can achieve that the wave speed in the homogeneous exterior domain $\mathbb{R}^d \backslash \overline{\Omega}$ is given by $c = 1$. The equations for the scattered field u excited by an incident wave u^{inc} are

as follows [20, Section 1.5]

(1.1)
$$\begin{cases} \dfrac{\partial^2 u}{\partial t^2}(\boldsymbol{x},t) - \Delta u(\boldsymbol{x},t) = 0, & \boldsymbol{x} \in \mathbb{R}^d \backslash \overline{\Omega} \;\; (\text{or} \;\; \boldsymbol{x} \in \Omega), \;\; t \geq 0, \\[2mm] u(\boldsymbol{x},t) = -u^{\text{inc}}(\boldsymbol{x},t), & \boldsymbol{x} \in \Gamma := \partial\Omega, \hspace{3.2cm} t \geq 0, \\[2mm] u(\boldsymbol{x},0) = \dfrac{\partial u}{\partial t}(\boldsymbol{x},0) = 0, & \boldsymbol{x} \in \mathbb{R}^d \backslash \overline{\Omega} \;\; (\text{or} \;\; \boldsymbol{x} \in \Omega). \end{cases}$$

This is a wave equation with Dirichlet boundary conditions and zero initial conditions. At an initial time $t = 0$ it is assumed that the incident field has not yet reached the scatterer, which is reflected by our initial conditions.

Fundamental solutions for the wave equation in two and three dimensions centered at a given point $\boldsymbol{y} \in \Omega$ are the following

(1.2)
$$\mathcal{G}(\boldsymbol{x} - \boldsymbol{y}, t) = \begin{cases} \dfrac{H(t - |\boldsymbol{x} - \boldsymbol{y}|)}{2\pi\sqrt{t^2 - |\boldsymbol{x} - \boldsymbol{y}|^2}}, & d = 2, \\[4mm] \dfrac{\delta(t - |\boldsymbol{x} - \boldsymbol{y}|)}{4\pi|\boldsymbol{x} - \boldsymbol{y}|}, & d = 3. \end{cases}$$

The study of retarded potential integral operators based on (1.2) started with the work of Bamberger and Ha Duong [9], where they established the analysis in time-domain by means of Laplace Transform techniques. Galerkin Boundary Element methods were studied later in [11, 1]. Alternative numerical methods for retarded potentials based on collocation schemes can also be found in [8].

The exterior acoustic scattering problem has been efficiently solved in [3] by means of the convolution quadrature method and the boundary element method. We propose an alternative method based on convolution quadrature combined with the method of fundamental solutions, which is easy to implement and produces accurate numerical results.

2. Numerical Scheme.

2.1. Convolution Quadrature. We briefly describe the CQ-approach to the initial boundary value problem (1.1). We start with the wave equation, boundary conditions and initial conditions and derive frequency-domain problems based on multistep and multistage methods. Further details can be found in [14, Chapters 3, 4 and 6] and [20, Section 4].

We start by rewriting (1.1) as a first-order system in time. Let $v(\boldsymbol{x},t) := \dfrac{\partial u}{\partial t}(\boldsymbol{x},t)$ and define

(2.1)
$$U(\boldsymbol{x},t) := (u(\boldsymbol{x},t), v(\boldsymbol{x},t)).$$

From (1.1) it is clear that U satisfies

(2.2)
$$\begin{aligned} \frac{\partial U}{\partial t}(\boldsymbol{x},t) &= \mathcal{L}U(\boldsymbol{x},t), & \boldsymbol{x} \in \mathbb{R}^d \backslash \overline{\Omega}, \; t \geq 0, \\[2mm] U(\boldsymbol{x},t) &= -U^{\text{inc}}(\boldsymbol{x},t), & \boldsymbol{x} \in \Gamma := \partial\Omega, \; t \geq 0, \\[2mm] U(\boldsymbol{x},0) &= \boldsymbol{0}, & \boldsymbol{x} \in \mathbb{R}^d \backslash \overline{\Omega}, \end{aligned}$$

where $\mathcal{L} := \begin{pmatrix} 0 & I \\ \Delta & 0 \end{pmatrix}$ and $U^{\mathrm{inc}}(\boldsymbol{x}, t) := \left(u^{\mathrm{inc}}(\boldsymbol{x}, t), \dfrac{\partial u^{\mathrm{inc}}}{\partial t}(\boldsymbol{x}, t) \right).$

The system (2.2) can be discretized in time by multistep or multistage methods. Transforming the resulting equations in the Laplace domain will lead to the corresponding CQ scheme and will be explained in the following sections.

2.2. Multistep Convolution Quadrature. A multistep method for solving equation (2.2) is defined by parameters $\alpha_\ell, \beta_\ell \in \mathbb{R}$, $\ell = 0, \ldots, m$ and a time step $\Delta t > 0$ [22, Ch. III.2]. At discrete times $t_n := n\Delta t$, $n \in \mathbb{N}$ it generates approximations $U_n(\boldsymbol{x}) \approx U(\boldsymbol{x}, t_n)$ by the recursion

$$
(2.3) \qquad \sum_{\ell=0}^{m} \alpha_\ell U_{n+\ell-m} = \Delta t \sum_{\ell=0}^{m} \beta_\ell \mathcal{L} U_{n+\ell-m}, \quad n = 0, 1, \ldots.
$$

where we set $U_n = 0$ for $n \le 0$. Applying the Z-Transform [14, Sec. 2.2]

$$
(2.4) \qquad \boldsymbol{U}(\boldsymbol{x}, \zeta) := \sum_{n=0}^{\infty} U_n(\boldsymbol{x})\zeta^n = \sum_{n=0}^{\infty} (u_n(\boldsymbol{x}), v_n(\boldsymbol{x}))\zeta^n, \quad \zeta \in \mathbb{C}, \ |\zeta| < 1,
$$

on (2.3) leads to a new equation in the Z-domain that corresponds to

$$
(2.5) \qquad \frac{\delta(\zeta)}{\Delta t} \boldsymbol{U}(\boldsymbol{x}, \zeta) = \mathcal{L} \boldsymbol{U}(\boldsymbol{x}, \zeta), \quad \zeta \in \mathbb{C}, |\zeta| < 1
$$

where $\delta(\zeta) := \dfrac{\sum_{\ell=0}^{m} \alpha_{m-\ell} \zeta^\ell}{\sum_{\ell=0}^{m} \beta_{m-\ell} \zeta^\ell}$. We also obtain boundary conditions in the Z-domain,

$$
(2.6) \qquad \boldsymbol{U}(\boldsymbol{x}, \zeta) = -\boldsymbol{U}^{\mathrm{inc}}(\boldsymbol{x}, \zeta) := -\sum_{n=0}^{\infty} U^{\mathrm{inc}}(\boldsymbol{x}, t_n)\zeta^n, \quad \boldsymbol{x} \in \Gamma.
$$

Finally, we arrive at the following 1-parameter family of boundary value problems

$$
(2.7) \qquad \begin{aligned}
\frac{\delta(\zeta)}{\Delta t} \boldsymbol{U}(\boldsymbol{x}, \zeta) &= \mathcal{L} \boldsymbol{U}(\boldsymbol{x}, \zeta), & \boldsymbol{x} \in \mathbb{R}^d \backslash \overline{\Omega}, \quad |\zeta| < 1, \\
\boldsymbol{U}(\boldsymbol{x}, \zeta) &= -\boldsymbol{U}^{\mathrm{inc}}(\boldsymbol{x}, \zeta), & \boldsymbol{x} \in \Gamma, \quad |\zeta| < 1.
\end{aligned}
$$

Recalling that $\boldsymbol{U}(\boldsymbol{x}, \zeta) = (\boldsymbol{u}(\boldsymbol{x}, \zeta), \boldsymbol{v}(\boldsymbol{x}, \zeta))$, where

$$
(2.8) \qquad \frac{\delta(\zeta)}{\Delta t} \boldsymbol{v}(\boldsymbol{x}, \zeta) = \Delta \boldsymbol{u}(\boldsymbol{x}, \zeta), \quad \boldsymbol{x} \in \mathbb{R}^d \backslash \overline{\Omega}, |\zeta| < 1,
$$

leads to the following Helmholtz type boundary value problems

$$
(2.9) \qquad \begin{aligned}
-\Delta \boldsymbol{u}(\boldsymbol{x}, \zeta) - \left(i \frac{\delta(\zeta)}{\Delta t} \right)^2 \boldsymbol{u}(\boldsymbol{x}, \zeta) &= 0, & \boldsymbol{x} \in \mathbb{R}^d \backslash \overline{\Omega}, \quad |\zeta| < 1, \\
\boldsymbol{u}(\boldsymbol{x}, \zeta) &= -\boldsymbol{u}^{\mathrm{inc}}(\boldsymbol{x}, \zeta), & \boldsymbol{x} \in \Gamma, \quad |\zeta| < 1,
\end{aligned}
$$

with complex wavenumbers $k(\zeta) = i\dfrac{\delta(\zeta)}{\Delta t}$. Using an A-stable multistep method will ensure that the rational polynomial δ satisfies $\delta(\zeta) \in \mathbb{C}_+$ for $\zeta \in \mathbb{C}_+$ [17, Section 1, p.131]. However, we are interested in the time-domain solution $u(\boldsymbol{x}, t)$, not in the Z-domain solution $\boldsymbol{u}(\boldsymbol{x}, \zeta)$. Both of them are related by means of the inverse Z-Transform, which corresponds to an application of the Cauchy integral formula:

$$(2.10) \qquad u(\boldsymbol{x}, t_n) \approx u_n(\boldsymbol{x}) = \frac{1}{2\pi i} \int_{\mathcal{C}} \frac{\boldsymbol{u}(\boldsymbol{x}, \zeta)}{\zeta^{n+1}} \mathrm{d}\zeta, \quad \boldsymbol{x} \in \mathbb{R}^d \backslash \overline{\Omega}.$$

For implementation purposes, a good choice for the contour of integration $\mathcal{C}$ is a circle of radius $\lambda < 1$, which allows the use of the Fast Fourier Transform (FFT) to compute the integral approximately by means of a trapezoidal rule. Following [14, Section 4.2.1], the final expression is

$$(2.11) \qquad \frac{1}{2\pi i} \int_{\mathcal{C}} \frac{1}{\zeta^{n+1}} \boldsymbol{u}(\boldsymbol{x}, \zeta) \mathrm{d}\zeta \approx \frac{\lambda^{-n}}{N+1} \sum_{\ell=0}^{N} \boldsymbol{u}(\boldsymbol{x}, \zeta_\ell)\zeta_\ell^{-n}$$

where $\zeta_\ell := e^{\frac{2\pi i \ell}{N+1}}$, $\ell = 0, \dots, N$, and $N + 1 \in \mathbb{N}$ is the number of quadrature points in the trapezoidal rule. This means that we need to solve $N + 1$ frequency domain problems (2.9) with $\zeta = \zeta_\ell$, $\ell = 0, \dots, N$ to approximate the solution of our wave equation. The order of convergence of this method is the same as that of the multistep method chosen. Due to Dahlquist's Barrier Theorem [21, Chapter V, Theorem 1.4], A-stable multistep methods are limited to order ≤ 2, which is a major drawback of multistep-based CQ.

2.3. Multistage Convolution Quadrature. There are A-stable implicit multistage methods of arbitrary order [2]. This is the main motivation for considering them for solving (2.2) instead of multistep methods. Writing $\dfrac{\boldsymbol{c} \;\big|\; A}{\;\;\big|\; \boldsymbol{b}^T}$, $A \in \mathbb{R}^{m \times m}$, $\boldsymbol{b}, \boldsymbol{c} \in \mathbb{R}^m$, $m \in \mathbb{N}$ for the Butcher tableau for a given m-stage Runge-Kutta method, and defining the stages $U_{nj}(\boldsymbol{x}) \approx U(\boldsymbol{x}, t_n + c_j \Delta t)$ and the steps $U_n(\boldsymbol{x}) \approx U(\boldsymbol{x}, t_n)$, the method amounts to computing a sequence of vector valued functions

$$(2.12) \qquad \begin{aligned} \underline{U}_n(\boldsymbol{x}) \;\; &:= \;\; (U_{n1}(\boldsymbol{x}), \dots, U_{nm}(\boldsymbol{x})) \\ &= \;\; (U(\boldsymbol{x}, t_n + c_1 \Delta t), \dots, U(\boldsymbol{x}, t_n + c_m \Delta t)), \quad n = 0, \dots, N, \end{aligned}$$

of stage solutions such that

$$(2.13) \qquad \begin{aligned} \underline{U}_n \;\; &= \;\; U_n \boldsymbol{1} \;\; + \;\; \Delta t \, A \underline{\mathcal{L}} \, \underline{U}_n, \\ U_{n+1} \;\; &= \;\; U_n \;\; + \;\; \Delta t \, \boldsymbol{b} \cdot \underline{\mathcal{L}} \, \underline{U}_n. \end{aligned}$$

where $\underline{\mathcal{L}} \, \underline{U}_n := (\mathcal{L}U_{n1}(\boldsymbol{x}), \dots, \mathcal{L}U_{nm}(\boldsymbol{x}))$ and $\underline{U}_n = 0$, $U_n = 0$ for $n \leq 0$.
For stiffly accurate Runge-Kutta methods such as RadauIIA or LobattoIIIC families [19], we have the relation

$$\boldsymbol{e}_m^T A = \boldsymbol{b}^T,$$

where $e_m = (0, \dots, 0, 1) \in \mathbb{R}^m$. Thus, the second equation in (2.13) can be derived from the first one by multiplying from the left by $\boldsymbol{e}_m^T$. Then, we get the simpler recursion

$$(2.14) \qquad \underline{U}_n \;\; = \;\; \boldsymbol{1} \boldsymbol{e}_m^T \underline{U}_{n-1} \;\; + \;\; \Delta t \, A \underline{\mathcal{L}} \, \underline{U}_n,$$

The application of the Z-transform to this equation leads to the following equation in the Z-domain:

$$(2.15) \qquad \underline{\boldsymbol{U}}(\zeta) \;=\; \zeta \mathbf{1} \boldsymbol{e}_m^T \underline{\boldsymbol{U}}(\zeta) \;+\; \Delta t \, A \underline{\mathcal{L}} \, \underline{\boldsymbol{U}}(\zeta), \quad \zeta \in \mathbb{C}, \; |\zeta| < 1,$$

where we denote $\underline{\boldsymbol{U}}(\zeta) := \sum_{n=0}^{\infty} \underline{\boldsymbol{U}}_n \zeta^n = \displaystyle\sum_{n=0}^{\infty} ((u_{n1}(\boldsymbol{x}), v_{n1}(\boldsymbol{x})), \dots, (u_{nm}(\boldsymbol{x}), v_{nm}(\boldsymbol{x}))) \zeta^n$.

From (2.15) we obtain the following expression

$$(2.16) \qquad \frac{\boldsymbol{\delta}^{\mathrm{RK}}(\zeta)}{\Delta t} \, \underline{\boldsymbol{U}}(\zeta) \;=\; \underline{\mathcal{L}} \, \underline{\boldsymbol{U}}(\zeta),$$

where we wrote $\boldsymbol{\delta}^{\mathrm{RK}}(\zeta) := A^{-1} \left(I - \zeta \mathbf{1} \boldsymbol{e}_m^T \right) \in \mathbb{C}^{m \times m}$.

Similarly as for the multistep case, we derive a Helmholtz-type equation with a matrix-valued "wavenumber" of complex coefficients. Letting $\underline{\boldsymbol{U}} := ((\boldsymbol{u}_1, \boldsymbol{v}_1), \dots, (\boldsymbol{u}_m, \boldsymbol{v}_m))$, we define $\underline{\boldsymbol{u}} := (\boldsymbol{u}_1, \dots, \boldsymbol{u}_m)$ which satisfies the vector Helmholtz-type boundary value problems

$$(2.17) \qquad \begin{aligned} -\underline{\Delta} \, \underline{\boldsymbol{u}}(\boldsymbol{x}, \zeta) + \left(\frac{\boldsymbol{\delta}^{\mathrm{RK}}(\zeta)}{\Delta t} \right)^2 \underline{\boldsymbol{u}}(\boldsymbol{x}, \zeta) &= 0, & \boldsymbol{x} \in \mathbb{R}^d \backslash \overline{\Omega}, \\ \underline{\boldsymbol{u}}(\boldsymbol{x}, \zeta) &= -\underline{\boldsymbol{u}}^{\mathrm{inc}}(\boldsymbol{x}, \zeta), & \boldsymbol{x} \in \Gamma, \end{aligned} \qquad |\zeta| < 1,$$

where $\underline{\Delta} \, \underline{\boldsymbol{u}}(\boldsymbol{x}, \zeta) := (\Delta \boldsymbol{u}_1(\boldsymbol{x}, \zeta), \dots, \Delta \boldsymbol{u}_m(\boldsymbol{x}, \zeta))$. The system can be decoupled by diagonalization of the matrix-valued wavenumber

$$(2.18) \qquad \boldsymbol{\delta}^{\mathrm{RK}}(\zeta) = P(\zeta) D(\zeta) P^{-1}(\zeta),$$

where

$$(2.19) \qquad D(\zeta) = \mathrm{diag}(\delta_1^{\mathrm{RK}}(\zeta), \dots, \delta_m^{\mathrm{RK}}(\zeta)) \quad \text{and} \quad P(\zeta) \in \mathbb{C}^{m \times m}$$

are the matrices of eigenvalues and eigenvectors of $\boldsymbol{\delta}^{\mathrm{RK}}(\zeta)$, respectively. Finally, we need to solve for $j = 1, \dots, m$

$$(2.20) \qquad \begin{aligned} -\Delta \boldsymbol{w}_j(\boldsymbol{x}, \zeta) - \left(i \frac{\delta_j^{\mathrm{RK}}(\zeta)}{\Delta t} \right)^2 \boldsymbol{w}_j(\boldsymbol{x}, \zeta) &= 0, & \boldsymbol{x} \in \mathbb{R}^d \backslash \overline{\Omega}, \\ \boldsymbol{w}_j(\boldsymbol{x}, \zeta) &= -\boldsymbol{w}_j^{\mathrm{inc}}(\boldsymbol{x}, \zeta), & \boldsymbol{x} \in \Gamma, \end{aligned} \qquad |\zeta| < 1,$$

where we have used the change of variables $\underline{\boldsymbol{w}}(\boldsymbol{x}, \zeta) = P^{-1}(\zeta) \underline{\boldsymbol{u}}(\boldsymbol{x}, \zeta)$. As regards implementation, the procedure follows exactly that of (2.11), using the FFT and solving a finite number of Helmholtz-type boundary value problems.

2.4. Method of Fundamental Solutions. In the previous section, by means of the Z transform we reduced the time domain wave equation with Dirichlet boundary conditions to multiple Helmholtz Dirichlet boundary value problems. Different solvers in frequency domain can be used for these boundary value problems (BVPs). Here we focus on the Method of Fundamental Solutions. We are interested in solving either the interior or exterior Helmholtz Dirichlet BVP with wavenumber $k \in \mathbb{C}_+$ and Dirichlet boundary conditions, i.e.

$$(2.21) \qquad \begin{aligned} -\Delta u(\boldsymbol{x}) - k^2 u(\boldsymbol{x}) &= 0, & \boldsymbol{x} \in \Omega, \\ u(\boldsymbol{x}) &= g(\boldsymbol{x}), & \boldsymbol{x} \in \Gamma \end{aligned}$$

for the interior problem, or

$$
\begin{aligned}
-\Delta u(\boldsymbol{x}) - k^2 u(\boldsymbol{x}) &= 0, & \boldsymbol{x} \in \mathbb{R}^d \backslash \overline{\Omega}, \\
u(\boldsymbol{x}) &= g(\boldsymbol{x}), & \boldsymbol{x} \in \Gamma
\end{aligned}
$$
$$+\text{Radiation Conditions}$$

(2.22)

for the exterior problem. In both cases, g is a function defining Dirichlet boundary conditions, and models an incident field e.g a plane wave or a field generated by a point source.

As indicated by its name the MFS approximates u by a linear superposition of fundamental solutions. The fundamental solution for the Helmholtz equation in $\mathbb{R}^2$ is the Hankel function of the first kind and order zero

(2.23)
$$
G(\boldsymbol{x}, \boldsymbol{y}; k) := \frac{i}{4} H_0^{(1)}(k|\boldsymbol{x} - \boldsymbol{y}|), \quad \boldsymbol{x} \neq \boldsymbol{y}, \quad k \in \mathbb{C}.
$$

The Method of Fundamental Solutions (MFS) selects a finite set of points $\{\boldsymbol{y}_j\}_{j=1}^N$ and writes $\tilde{u}$ as a linear combination of fundamental solutions centered at these points

(2.24)
$$
\tilde{u}(\boldsymbol{x}) = \sum_{j=1}^{N_y} \alpha_j G(\boldsymbol{x}, \boldsymbol{y}_j; k), \quad \boldsymbol{x} \in \mathbb{R}^2 \backslash \overline{\Omega},
$$

with coefficients $\alpha_j \in \mathbb{C}$, $j = 1, \ldots, N_y$. In 2D, the source locations $\{\boldsymbol{y}_j\}$ are chosen on a smooth curve contained in the domain Ω for exterior problems, and enclosing Ω for interior problems (see Figure 1). Exponential convergence can be achieved if these are suitable chosen for analytic domains [4]. The optimal placement of auxiliary sources is still an unsolved problem in 3D.
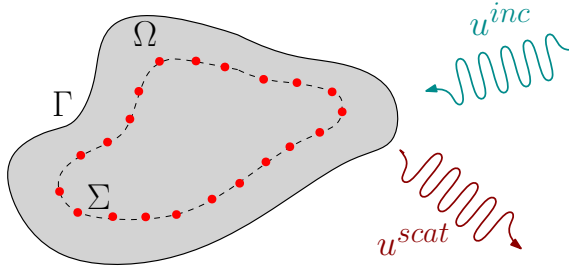

Fig. 1: Example geometry with source points (red dots) inside Ω on curve Σ (dashed line).

The coefficients can be determined by $L^2(\Gamma)$-fitting of the known boundary data g, thus enforcing the Dirichlet boundary conditions. We need to find coefficients α_j, $j = 1, \ldots, N$, such that, with $\tilde{u}$ as in (2.24)

(2.25)
$$
(\alpha_1, \ldots, \alpha_N) = \operatorname{argmin}_{\boldsymbol{\alpha} \in \mathbb{C}^N} \|\tilde{u} - g\|_{L^2(\Gamma)}.
$$

This can be done by choosing quadrature points $\boldsymbol{x}_\ell$, $\ell = 1, \ldots, N_x$, to approximate the L^2-norm on the boundary. Then, the problem can be solved by a least squares method. We can rewrite it

in matrix form as

$$
(2.26) \qquad\qquad \boldsymbol{\alpha}^{\star} = \mathrm{argmin}_{\boldsymbol{\alpha}\in\mathbb{C}^{N}} \|\mathbb{M}\boldsymbol{\alpha} - \boldsymbol{g}\|_{2}.
$$

where $\boldsymbol{\alpha} = (\alpha_{1},\ldots,\alpha_{N_{y}})^{T}$, $\boldsymbol{g} = (g(\boldsymbol{x}_{1}),\ldots,g(\boldsymbol{x}_{N_{x}}))^{T}$ and $\mathbb{M}_{\ell j} = G(\boldsymbol{x}_{\ell},\boldsymbol{y}_{j};k)$ for $\ell = 1,\ldots,N_{x},\ j = 1,\ldots,N_{y}$.

3. Algorithm. We denote

$$
(3.1) \qquad \mathbb{M}(\zeta) := \begin{pmatrix} G(\boldsymbol{x}_{0},\boldsymbol{y}_{0};\zeta) & \ldots & G(\boldsymbol{x}_{0},\boldsymbol{y}_{N_{y}};\zeta) \\ \vdots & \ldots & \vdots \\ G(\boldsymbol{x}_{N_{x}},\boldsymbol{y}_{0};\zeta) & \ldots & G(\boldsymbol{x}_{N_{x}},\boldsymbol{y}_{N_{y}};\zeta) \end{pmatrix} \in \mathbb{C}^{N_{x}\times N_{y}}
$$

the matrix related to the minimization problem arising from the MFS (2.25). Note that this is a dense matrix. Concerning the selection of source points we follow [15, 4]. For the two dimensional Helmholtz equation over a domain $\Omega \subset \mathbb{R}^{2}$ with analytic boundary Γ let $\Phi : \mathbb{C} \to \mathbb{C}$ be such that

$$
(3.2) \qquad \Gamma := \{\boldsymbol{x} \in \mathbb{R}^{2}\ :\ \boldsymbol{x} = (\mathrm{Re}\ \Phi(z), \mathrm{Im}\ \Phi(z)), \quad z \in \mathbb{C}, \quad |z| = 1\}
$$

and

$$
(3.3) \qquad \Sigma := \{\boldsymbol{x} \in \mathbb{R}^{2}\ :\ \boldsymbol{x} = (\mathrm{Re}\ \Phi(z), \mathrm{Im}\ \Phi(z)), \quad z \in \mathbb{C}, \quad |z| = r\}
$$

are the boundary Γ of the domain Ω and the curve Σ where charge points are chosen, respectively. The fixed parameter $0 < r < 1$ (resp. $r > 1$) for exterior (resp. interior) problems. This was proposed for the Laplace problem [15] and has been used for Helmholtz problems too. In [4] a different approach is suggested to improve results in the presence of singularities in the parametrizations of analytic domains, but for simplicity we decided not to use it, because our focus is on testing the direct coupling of CQ and MFS.

We present the algorithms for the multistep and multistage case. The CQ implementation is mainly based on the presentation given in [14, Sections 4 and 6]. It is worth mentioning that a scaling of the data is needed in order to correctly compute the Z-Transform of boundary data and the inverse Z-Transform as a contour integral over a circle of radius $0 < \lambda < 1$ [14, Section 4.2]. Evaluating Z-Transforms at points $\zeta_{\ell} = \lambda \exp\left(\frac{2\pi i\ell}{M+1}\right)$ is equivalent to computing the Discrete Fourier Transform (DFT) of scaled functions:

$$
(3.4) \qquad \sum_{n=0}^{M} g(\boldsymbol{x},t_{n})\zeta_{\ell}^{n} = \sum_{n=0}^{M} \{\lambda^{n} g(\boldsymbol{x},t_{n})\} \exp\left(\frac{2\pi i\ell n}{M+1}\right).
$$

Also, computing the approximate contour integral of the inverse Z-Transform (2.11) is equivalent to computing an inverse DFT and rescaling the output:

$$
(3.5) \qquad u(\boldsymbol{x},t_{n}) \approx \frac{\lambda^{-n}}{N+1} \sum_{\ell=0}^{M} \boldsymbol{u}(\boldsymbol{x},\zeta_{\ell})\zeta_{\ell}^{-n} = \lambda^{-n}\left(\frac{1}{M+1} \sum_{\ell=0}^{M} \boldsymbol{u}(\boldsymbol{x},\zeta_{\ell})\exp\left(\frac{-2\pi i\ell n}{M+1}\right)\right).
$$

Observe that this involves using the same number of quadrature points for the trapezoidal rule in (3.5) as the number of discrete times $t_{n}, n = 0,\ldots,M$. As we are dealing with analytic functions

(Helmholtz solutions for $k \in \mathbb{C}_+$) this is not a problem, as exponential convergence is guaranteed for the trapezoidal rule. Nevertheless, some experiments have shown that accuracy can be lost in presence of cavities, due to the appearence of so-called scattering poles [5], making it necessary to overresolve in the frequency domain.

Now, we give details of the algorithms used for the multistep and multistage CQ combined with MFS. The computational complexity of these algorithms is mainly due to solving the linear system by a least squares method. Boundary data can be stored in a matrix of size $N_x \times M$. The cost of computing the DFT by means of the FFT is negligible compared to the other steps. The assembly of a single matrix requires $\mathcal{O}(N_x N_y)$ operations, because it involves evaluations over charge and collocation points. The least squares problem is solved by the QR method for a dense matrix (based on Matlab's backslash operator) which is the most costly operation in the algorithm. This is repeated M times, where M is the number of timesteps. For the case of Runge-Kutta methods, this has to be multiplied by the number of stages m.

Multistep CQ - MFS

a) Define $\lambda = \epsilon^{1/2M}$ and $\Delta t = T/M$.

b) For a given parametrization $\Phi : \mathbb{C} \mapsto \mathbb{C}$ and some $r \in (0,1)$ compute

(3.6)
$$\boldsymbol{x}_\ell = (\text{Re } \Phi(z_\ell), \text{Im } \Phi(z_\ell)), \qquad z_\ell = \exp\left(\frac{2i\ell\pi}{N_x+1}\right), \ \ell = 0, \ldots, N_x,$$

$$\boldsymbol{y}_j = (\text{Re } \Phi(rz_j), \text{Im } \Phi(rz_j)), \quad z_j = \exp\left(\frac{2ij\pi}{N_y+1}\right), \ \ell = 0, \ldots, N_y.$$

c) Compute the data

(3.7)
$$g(\boldsymbol{x}_\ell, t_n) = -u^{\text{inc}}(\boldsymbol{x}_\ell, t_n), \quad \ell = 0, \ldots, N_x, \ n = 0, \ldots, M.$$

d) Rescale the data:

(3.8)
$$h_n(\boldsymbol{x}_\ell) = \lambda^n g(\boldsymbol{x}_\ell, t_n), \quad \ell = 0, \ldots, N_x, \ n = 0, \ldots, M.$$

e) Compute the DFT of the scaled data $\{h_n(\boldsymbol{x}_\ell)\}_{n=0}^M$, $\ell = 0, \ldots, N_x$, to obtain

(3.9)
$$\{\tilde{h}_n(\boldsymbol{x}_\ell)\}_{n=0}^M, \quad \ell = 0, \ldots, N_x.$$

f) For each $n = 0, \ldots, M$, solve the least squares problem to obtain the vector of coefficients:

(3.10)
$$\boldsymbol{\alpha}^\star(\zeta_n) = \text{argmin}_{\boldsymbol{\alpha} \in \mathbb{C}^{N_y+1}} \left\| \mathbb{M}(\delta(\zeta_n)/\Delta t)\boldsymbol{\alpha} - \widetilde{\boldsymbol{h}}_n \right\|_2$$

where $\boldsymbol{\alpha} := \begin{pmatrix} \alpha_0 & \cdots & \alpha_{N_y} \end{pmatrix}^T$, $\widetilde{\boldsymbol{h}}_n := \begin{pmatrix} \tilde{h}_n(\boldsymbol{x}_0) & \cdots & \tilde{h}_n(\boldsymbol{x}_{N_x}) \end{pmatrix}^T$ and $\mathbb{M}(\delta(\zeta_n)/\Delta t)$ is defined by (3.1).

g) Evaluate the solutions in a prescribed set of points of interest $\{\boldsymbol{p}_l\}_{l=0}^{N_p}$

(3.11)
$$\widetilde{v}_n(\boldsymbol{p}_l) = \sum_{j=0}^{N_y} \alpha_j^\star(\zeta_n) G(\boldsymbol{p}_l - \boldsymbol{y}_j; k_n)$$

to obtain the vector $\widetilde{\boldsymbol{v}}_n = \begin{pmatrix} \widetilde{v}_n(\boldsymbol{p}_0) & \cdots & \widetilde{v}_n(\boldsymbol{p}_{N_p}) \end{pmatrix}^T$

h) Compute the inverse DFT over the rows of the matrix $\widetilde{v} = \begin{pmatrix} \widetilde{v}_0 & \dots & \widetilde{v}_M \end{pmatrix}$ to obtain

$$(3.12) \qquad\qquad \boldsymbol{v} = \begin{pmatrix} \boldsymbol{v}_0 & \dots & \boldsymbol{v}_M \end{pmatrix}.$$

i) Finally, rescale the solution to recover the approximations

$$(3.13) \qquad\qquad u(\boldsymbol{p}_l, t_n) \approx \lambda^{-n} v_n(\boldsymbol{p}_l), \quad l = 0, \dots, N_p, \quad n = 0, \dots, M.$$

Multistage CQ - MFS

a) Define $\lambda = \epsilon^{1/2M}$ and $\Delta t = T/M$.

b) For a given parametrization $\Phi : \mathbb{C} \mapsto \mathbb{C}$ and $r \in (0,1)$ compute:

$$\boldsymbol{x}_\ell \quad \text{for} \quad \ell = 0, \dots, N_x, \quad \boldsymbol{y}_j \quad \text{for} \quad j = 0, \dots, N_y$$

as in (3.6).

c) Compute the data for each stage $s = 1, \dots, S$

$$(3.14) \qquad g(\boldsymbol{x}_\ell, t_n + c_s \Delta t) = -u^{\mathrm{inc}}(\boldsymbol{x}_\ell, t_n + c_s \Delta t), \quad \ell = 0, \dots, N_x, \ n = 0, \dots, M.$$

d) Rescale the data:

$$(3.15) \qquad h_{n,s}(\boldsymbol{x}_\ell) = \lambda^n g(\boldsymbol{x}_\ell, t_n + c_s \Delta t), \quad \ell = 0, \dots, N_x, \ n = 0, \dots, M.$$

e) Compute the DFT of the scaled data $\{h_{n,s}(\boldsymbol{x}_\ell)\}_{n=0}^M$, $\ell = 0, \dots, N_x$, $s = 1, \dots, m$, to obtain

$$(3.16) \qquad \tilde{h}_s := \{\tilde{h}_{n,s}(\boldsymbol{x}_\ell)\}_{n=0}^M, \quad \ell = 0, \dots, N_x, \quad s = 1, \dots, m$$

and denote

$$(3.17) \qquad \widetilde{\boldsymbol{h}}_n := \left(\tilde{h}_{n,1}(\boldsymbol{x}_0), \dots, \tilde{h}_{n,1}(\boldsymbol{x}_{N_x}), \dots, \tilde{h}_{n,m}(\boldsymbol{x}_0), \dots, \tilde{h}_{n,m}(\boldsymbol{x}_{N_x})\right)^T.$$

f) For each $n = 0, \dots, M$ compute the diagonalization (2.18):

$$\delta^{\mathrm{RK}}(\zeta_n) = P(\zeta_n) D(\zeta_n) P^{-1}(\zeta_n)$$

and the Kronecker product

$$P^{-1}(\zeta_n) \otimes \widetilde{\boldsymbol{h}}_n = \boldsymbol{\nu}_n = (\boldsymbol{\nu}_{n,1}, \dots, \boldsymbol{\nu}_{n,m}).$$

Then, for $s = 1, \dots, m$ solve the least squares problem to obtain the vector of coefficients:

$$(3.18) \qquad \boldsymbol{\alpha}_s^\star(\zeta_n) = \mathrm{argmin}_{\boldsymbol{\alpha} \in \mathbb{C}^{N_y+1}} \left\| \mathbb{M}(\delta_s^{\mathrm{RK}}(\zeta_n)/\Delta t)\boldsymbol{\alpha} - \boldsymbol{\nu}_{n,s} \right\|_2$$

where $\boldsymbol{\alpha} := \left(\alpha_0, \dots, \alpha_{N_y}\right)^T$ and $\mathbb{M}(\delta_s^{\mathrm{RK}}(\zeta_n)/\Delta t)$ is defined by (3.1).

g) Evaluate the solutions in a prescribed set of points of interest $\{\boldsymbol{p}_l\}_{l=0}^{N_p}$

$$(3.19) \qquad\qquad \widetilde{v}_{n,s}(\boldsymbol{p}_l) = \sum_{j=0}^{N_y} \alpha_{j,s}^\star(\zeta_n) G(\boldsymbol{p}_l - \boldsymbol{y}_j; i\delta_s^{\mathrm{RK}}(\zeta_n)/\Delta t)$$

to obtain the vector $\widetilde{\boldsymbol{v}}_{n,s} = \left(\widetilde{v}_{n,s}(\boldsymbol{p}_0) \quad \dots \quad \widetilde{v}_{n,s}(\boldsymbol{p}_{N_p})\right)^T$

h) Compute the Kronecker product

$$P(\zeta_n) \otimes (\widetilde{\boldsymbol{v}}_{n,1}, \ldots, \widetilde{\boldsymbol{v}}_{n,m}) = \widetilde{\widetilde{\boldsymbol{v}}}_n$$

i) Compute the inverse DFT over the rows of the matrix $\boldsymbol{V}_s = \left(\widetilde{\widetilde{\boldsymbol{v}}}_{0,s} \quad \ldots \quad \widetilde{\widetilde{\boldsymbol{v}}}_{M,s} \right)$ to obtain

(3.20) $$\boldsymbol{v}_s = \left(\boldsymbol{v}_{0,s} \quad \ldots \quad \boldsymbol{v}_{M,s} \right).$$

j) Finally, rescale the solution and get the approximation

(3.21) $$u(\boldsymbol{p}_l, t_n + \Delta t) \approx \lambda^{-n} v_{n,S}(\boldsymbol{p}_l), \quad l = 0, \ldots, N_p, \quad n = 0, \ldots, M.$$

4. Numerical Experiments. For all of our examples we will consider an incident field consisting of a plane wave, i.e. for a given $\boldsymbol{d} \in \mathbb{R}^2$ the incident field u^{inc} is given as

(4.1) $$u^{\mathrm{inc}}(\boldsymbol{x}, t) := f(t - t_{\mathrm{lag}} - \boldsymbol{d} \cdot \boldsymbol{x}), \quad \boldsymbol{x} \in \mathbb{R}^2, \ t \in \mathbb{R},$$

where

(4.2) $$f(t) := \sin(\omega t)\mu(t)\mu(4 - t), \quad \mu(t) := \frac{\exp(-\beta t)}{1 + \exp(-\beta t)}, \quad \beta = 5, \quad \omega = 4.$$

The errors are measured considering a relative pointwise error in space, discrete L^2-norm in time:

(4.3) $$\mathrm{error} := \frac{\left(\displaystyle\sum_{n=0}^{N} \sum_{\boldsymbol{p} \in X} |u(\boldsymbol{p}, t_n) - \tilde{u}(\boldsymbol{p}, t_n)|^2 \right)^{1/2}}{\left(\displaystyle\sum_{n=0}^{N} \sum_{\boldsymbol{p} \in X} |u(\boldsymbol{p}, t_n)|^2 \right)^{1/2}},$$

where $X \subset \mathbb{R}^2 \backslash \Omega$ is a finite set.

Multistep CQ is tested in two cases based on backward differentiation formulas (BDF) of order 1 and 2. Those are fully described by the following polynomials

(4.4) $$\delta^{\mathrm{BDF1}}(\zeta) = 1 - \zeta, \quad \delta^{\mathrm{BDF2}}(\zeta) = \frac{1}{2}\left(\zeta^2 - 4\zeta + 3 \right).$$

Multistage CQ is tested for the RadauIIA family, considering methods of two and three stages respectively. Their Butcher tableau is given by

(4.5) $$A = \begin{pmatrix} 5/12 & -1/12 \\ 3/4 & 1/4 \end{pmatrix}, \quad \boldsymbol{b}^T = \boldsymbol{e}_m^T A, \quad \boldsymbol{c} = A\boldsymbol{1},$$

for the two-stage method, and

(4.6)
$$A = \begin{pmatrix} 11/45 & 37/225 & -2/225 \\ 37/225 & 11/45 & -2/225 \\ 4/9 & 4/9 & 1/9 \end{pmatrix} + \begin{pmatrix} -7\frac{\sqrt{6}}{360} & -169\frac{\sqrt{6}}{1800} & \frac{\sqrt{6}}{75} \\ 169\frac{\sqrt{6}}{1800} & 7\frac{\sqrt{6}}{360} & -\frac{\sqrt{6}}{75} \\ -\frac{\sqrt{6}}{36} & \frac{\sqrt{6}}{36} & 0 \end{pmatrix}, \quad \boldsymbol{b}^T = \boldsymbol{e}_m^T A, \quad \boldsymbol{c} = A\boldsymbol{1},$$

for the three-stage method. RadauIIA families have classical order of convergence of $2m+1$, stage order of convergence of m, where m is the number of stages [21].

To take advantage of the exponentially decaying nature of the fundamental solutions for Im $k > 0$, we discard entries of matrix (3.1) that are below a given threshold of 10^{-20} as it was done in [7]. This allows us to use sparse linear solvers for most of our least squares problems, without losing accuracy. Our implementation was done in Matlab 2018a using the backslash operator, which solves the least squares problem by the QR method.

4.1. Method of Fundamental Solutions for complex wavenumbers. First, we need to validate that the method behaves correctly in this different setting. The problem studied is

(4.7)
$$\begin{aligned} -\Delta u(\boldsymbol{x}) - k^2 u(\boldsymbol{x}) &= 0 && \text{in } \mathbb{R}^2 \backslash \Omega, \\ u(\boldsymbol{x}) &= -u^{\text{inc}}(\boldsymbol{x}) && \text{on } \Gamma, \\ &+ \text{ Radiation Conditions} \end{aligned}$$

where Ω is the unit disk and source points are chosen on a circle of radius $r = 0.8$. The incident field $u^{\text{inc}}(\boldsymbol{x})$ corresponds to

(4.8)
$$u^{\text{inc}}(\boldsymbol{x}) = \frac{i}{4} H_0^{(1)}(k|\boldsymbol{x} - \boldsymbol{x}_{\text{src}}|), \quad \boldsymbol{x} \in \mathbb{R}^2,$$

where $\boldsymbol{x}_{\text{src}} = (0.2, 0.3)$. As this is an exterior problem and we are locating a source in the interior of the domain, the exact solution for the problem is $u(\boldsymbol{x}) = -u^{\text{inc}}(\boldsymbol{x})$ in the exterior of Ω.

The number of collocation points is $N = 600$ for each problem. Convergence results for the numerical experiments are shown in Figure 2. We observe exponential convergence for the MFS for several complex wavenumbers.

4.2. Scattering at a disk. Our first example consists in solving the interior problem of acoustic scattering at a disk of unit radius. The incident field is the plane wave defined in (4.1). We solve the interior problem with Dirichlet boundary conditions, for which we expect as a solution

(4.9)
$$u(\boldsymbol{x}, t) = u^{\text{inc}}(\boldsymbol{x}, t), \quad \boldsymbol{x} \in \mathbb{R}^2 \backslash \Omega.$$

The speed of propagation of the wave is always set to $c = 1$ and the final time of computation is $T = 10$.

Convergence of BDF1, BDF2 and RadauIIA Runge-Kutta methods is presented in Figure 3a. The number of collocation points and sources are chosen as rather large $N_x = 2000, N_y = 1000$ to have errors mainly due to the time discretization and not by the spatial error due to the MFS.
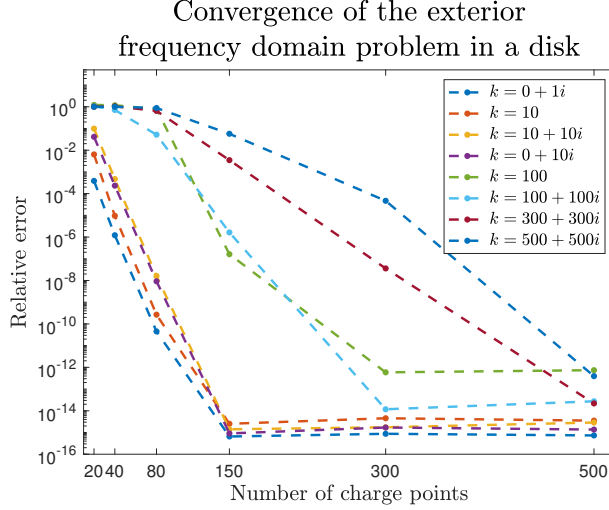
Fig. 2: Convergence results for the exterior Helmholtz problem of Section 4.1 with different wavenumbers.

Sources are located in a circle of radius $r = 1.2$.

The solution is computed at $X = \{(-0.5, -0.5), (-0.5, 0.5), (0.5, 0.5), (0.5, -0.5)\}$. We also solve the exterior problem and compare our results with respect to a highly resolved solution based on three stages RadauIIA method with $M = 1600$. The radius used for the curve Σ is $r = 0.8$ and the solution is computed in $X = \{(-2, -2), (-2, 2), (2, 2), (2, -2)\}$. Results are shown in Figure 3b. Both experiments show that it is possible to obtain the classical order of convergence of each multistep and multistage method, although for the interior problem a limited accuracy is reached, which was not possible to improve by increasing the number of charges. This can be explained by the limited accuracy that in general is achievable by the CQ method [14]. We also illustrate the percentage of matrix entries retained due to sparsification in Figure 5, for BDF2 based CQ with 1600 timesteps.

4.3. Scattering at a rounded triangle. We repeat the example of the previous section but with a different geometry. Now we consider a rounded triangle, which can be parametrized for $s \in [0, 2\pi]$

$$(4.10) \qquad x(s) + iy(s) = e^{is} + a_1 e^{-2is}, \quad a_1 = 0.3.$$

The complexification of this can be seen as $\Phi(z) = z + \dfrac{a_1}{z^2}$, $z \in \mathbb{C}$. If we restrict Φ to the unit circle we obtain $\Phi(e^{is}) = x(s) + iy(s)$. We define our geometries of interest by

$$(4.11) \qquad \Gamma := \{(x, y) \in \mathbb{R}^2 \ : \ x = x(s), \ y = y(s), \ \Phi(e^{is}) = x(s) + iy(s) \ \text{ for } s \in [0, 2\pi]\}$$

and

$$(4.12) \qquad \Sigma := \{(x, y) \in \mathbb{R}^2 \ : \ x = x(s), \ y = y(s), \ \Phi(re^{is}) = x(s) + iy(s) \ \text{ for } s \in [0, 2\pi]\},$$

(a) Interior problem.
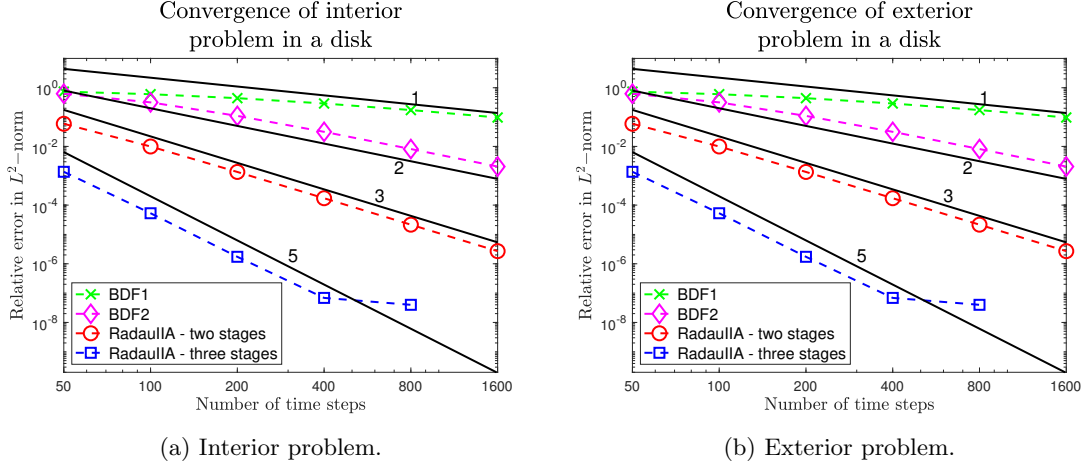
(b) Exterior problem.

Fig. 3: Convergence of the CQ scheme for the interior/exterior problem in Section 4.2, compared with an (a) exact solution; (b) highly resolved solution.

with the radius $r = 1.2$ for the interior problem and $r = 0.85$ for the exterior problem. These geometries are shown in Figure 6. Numerical results for this experiment are the same as for the unit circle, choosing fixed values $N = 2000, N_p = 1000$. The solution was computed in $X = \{(-0.5, -0.5), (-0.5, 0.5), (0, 0), (0.5, 0)\}$ for the interior problem and $X = \{(-2, -2), (-2, 2), (2, 2), (2, -2)\}$ for the exterior problem. Results are shown in Figures 7a and 7b, were the classical convergence rates are obtained.

4.4. Scattering at an inverted ellipse. We repeat the example with an inverted ellipse, which can be parametrized for $s \in [0, 2\pi]$

$$(4.13) \qquad x(s) + iy(s) = \frac{e^{is}}{1 + a_2 e^{2is}}, \quad a_2 = 0.25.$$

The complexification of this is $\Phi(z) = \dfrac{z}{1 + a_2 z^2}$, $z \in \mathbb{C}$. If we restrict Φ to the unit circle we obtain $\Phi(e^{is}) = x(s) + iy(s)$. We define our geometries of interest by

$$(4.14) \qquad \Gamma := \{(x, y) \in \mathbb{R}^2 \ : \ x = x(s), \ y = y(s), \ \Phi(e^{is}) = x(s) + iy(s) \ \text{ for } s \in [0, 2\pi]\}$$

and

$$(4.15) \qquad \Sigma := \{(x, y) \in \mathbb{R}^2 \ : \ x = x(s), \ y = y(s), \ \Phi(re^{is}) = x(s) + iy(s) \ \text{ for } s \in [0, 2\pi]\},$$

with the radius $r = 1.2$ for the interior problem and $r = 0.8$ for the exterior problem. These geometries are shown in Figure 9. Choosing fixed values $N = 2000, N_p = 1000$, the solution is computed in $X = \{(-0.5, -0.5), (-0.5, 0.5), (0.5, 0.5), (0.5, -0.5)\}$ for the interior problem, $X = \{(-2, -2), (-2, 2), (2, 2), (2, -2)\}$ for the exterior problem. Errors are shown in Figures 10a and 10b. Similar behavior as in the previous sections is observed, with classical order of convergence obtained.
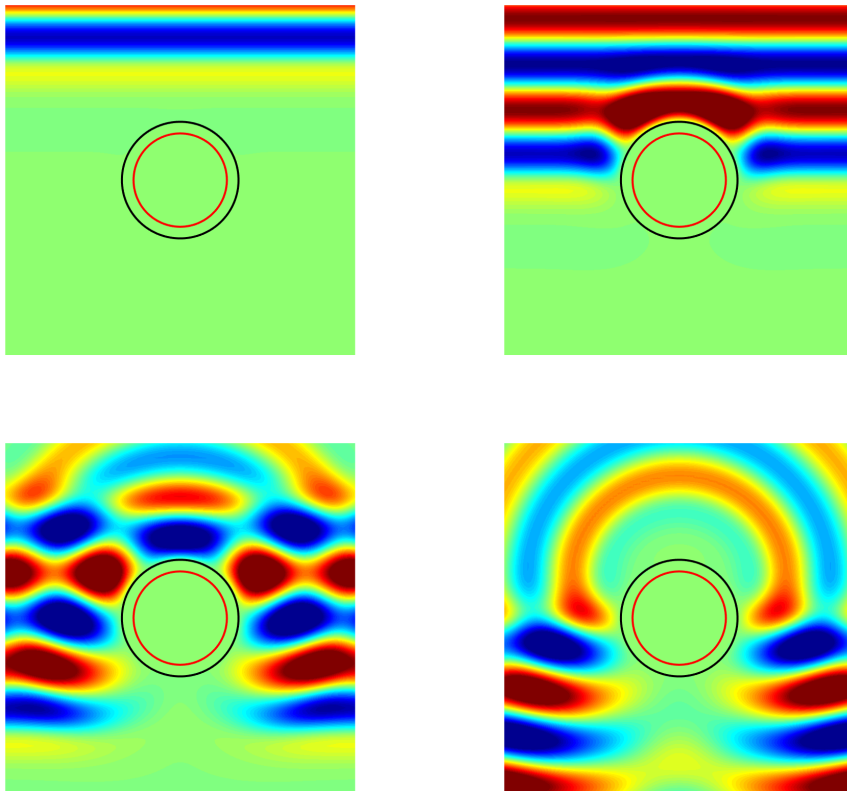
Fig. 4: Snapshots of the solution to the exterior problem in $[-3, 3] \times [-3, 3]$ at times $t = 2, 4, 6$ and 8.

4.5. Incident source close to scatterer. The proposed scheme suffers from inaccuracies in case of early-onset incident fields due to close sources. The situation is shown in Figure 12. Let us consider an incident field given by

$$(4.16) \qquad u^{\mathrm{inc}}(\boldsymbol{x}, t) := \int_0^t \mathcal{G}(\boldsymbol{x} - \boldsymbol{x}_{\mathrm{src}}, t - \tau) f(\tau) \, \mathrm{d}\tau,$$

where $\mathcal{G}(\boldsymbol{x}, t)$ is the fundamental solution of the wave equation defined in (1.2), $\boldsymbol{x}_{\mathrm{src}} \in \mathbb{R}^2$ is the location of the source and $f(t)$ is a signal in time. The position of $\boldsymbol{x}_{\mathrm{src}}$ determines the time that takes the incident field to reach the boundary Γ of the scatterer. Assuming the wavespeed to be $c = 1$ we obtain that

$$(4.17) \qquad u(\boldsymbol{x}^{\star}, t^{\star}) \neq 0$$
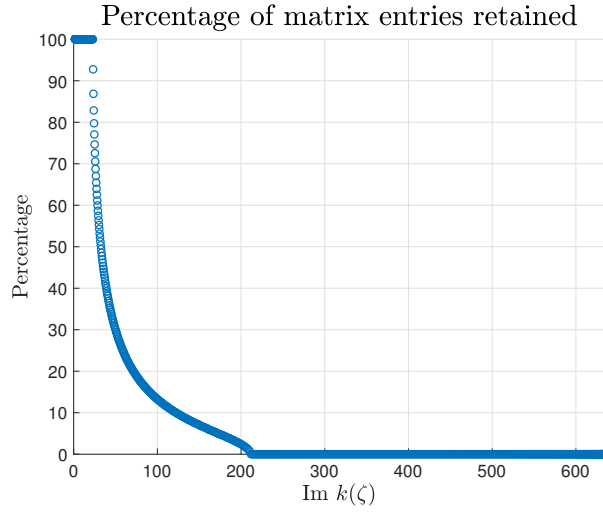
Fig. 5: Percentage of matrix entries (3.1) from experiment in Section 4.2 retained due to sparsification with tolerance 10^{-20} for BDF2 CQ with $M = 1600$.

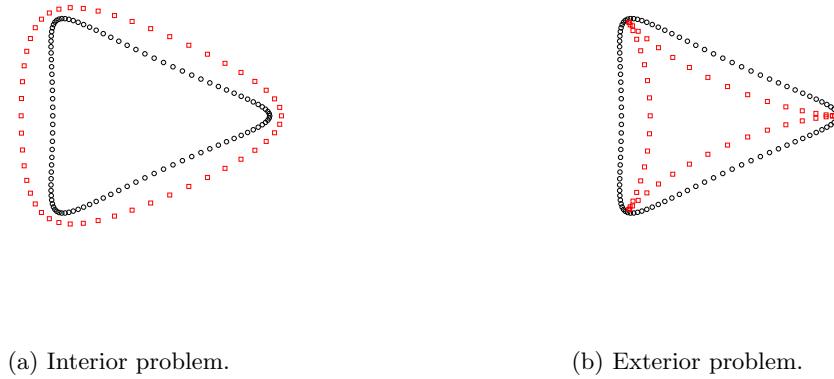(a) Interior problem.

(b) Exterior problem.

Fig. 6: Rounded triangle. Collocation points are marked as black circles, while charge points are marked as red squares. Interior and exterior problem, respectively

for some $t^\star > d(\boldsymbol{x}_{\mathrm{src}}, \Gamma)$ in a point $\boldsymbol{x}^\star \in \Gamma$. However, our approximation of $u(\boldsymbol{x}^\star, t^\star)$ given by $\tilde{u}(\boldsymbol{x}^\star, t^\star)$ from (2.24) depends on the auxiliary sources located on the curve Σ. For the case $d(\boldsymbol{x}^\star, \Sigma) > t^\star > d(\boldsymbol{x}_{\mathrm{src}}, \Gamma)$, signals from sources on Σ are not able to reach the boundary Γ at time $t^\star$ and our approximation turns out to be $\tilde{u}(\boldsymbol{x}^\star, t^\star) = 0$. This error propagates to the time stepping

(a) Interior problem.   (b) Exterior problem.
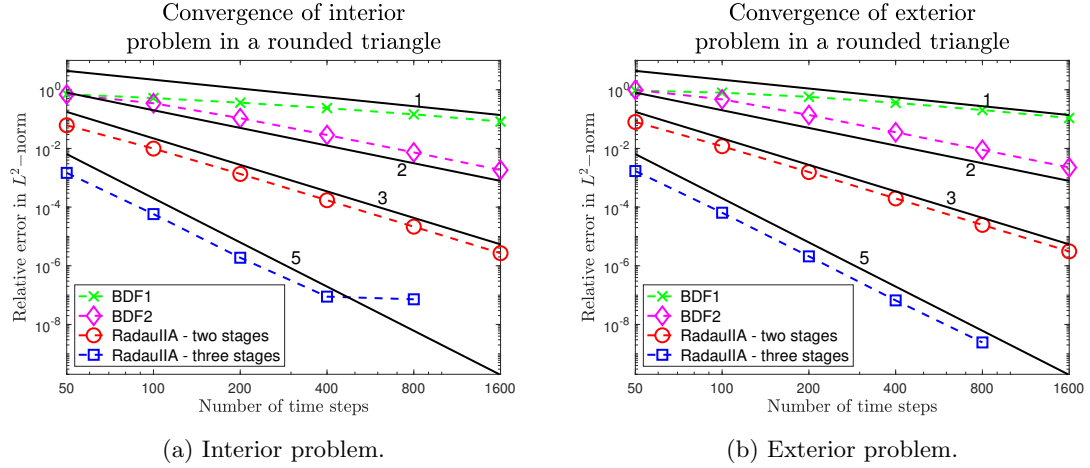
Fig. 7: Convergence of the CQ scheme for the interior/exterior problem in Section 4.3, compared with an (a) exact solution; (b) highly resolved solution.

scheme, leading to a wrong solution.

To illustrate this issue, let us consider the exterior scattering problem at a disk of unit radius and sources located in a circle of radius $r = 0.8$ as in Section 4.2. The incident field is given as in (4.16) with $\boldsymbol{x}_{\mathrm{src}} = (0, 0.95)$ and the signal is defined by

$$(4.18) \qquad\qquad f(t) := \sin(2t)^5 H(t), \quad t \in \mathbb{R},$$

where H is the Heavyside function. The exact solution of this problem is given by $u(\boldsymbol{x}, t) = u^{\mathrm{inc}}(\boldsymbol{x}, t)$. CQ-MFS applied as in Section 4.2 fails, see bold error line in Figure 13.

We found a simple remedy. It is enough to introduce a delay in the starting time of the signal f, replacing it by $\tilde{f}(t) = f(t - t_{\mathrm{lag}})$. We show the results of the numerical experiment for different values of t_{lag} in Figure 13. Strikingly, a simple delay in time of the incident field improves the accuracy of the solution. As pointed out, this has a simple physical explanation, the waves produced by auxiliary sources can reach the boundary before the incident field.

5. Conclusions. Throughout this article we worked with the Convolution Quadrature methods in combination with the Method of Fundamental Solutions as a frequency domain solver. Our numerical experiments on 2D analytic domains show that this combination performs well. We obtain classical orders of convergence for multistep and multistage methods at interior and exterior problems. The fundamental solutions of Helmholtz problems with complex wavenumbers are exponentially decaying for the case $k \in \mathbb{C}_+$, which gives us the opportunity to sparsify matrices. Our numerical tests show that this procedure is effective.

This work is a starting point: MFS is a representative of a larger class of Trefftz methods. A generalization is the Multiple Multipole Method [12]. It has been succesfully used for 3D frequency domain simulations based on heuristics for the placement of multipoles [13]. This work offers a proof of concept that CQ can be used to transfer these techniques to time domain. Possible ex-
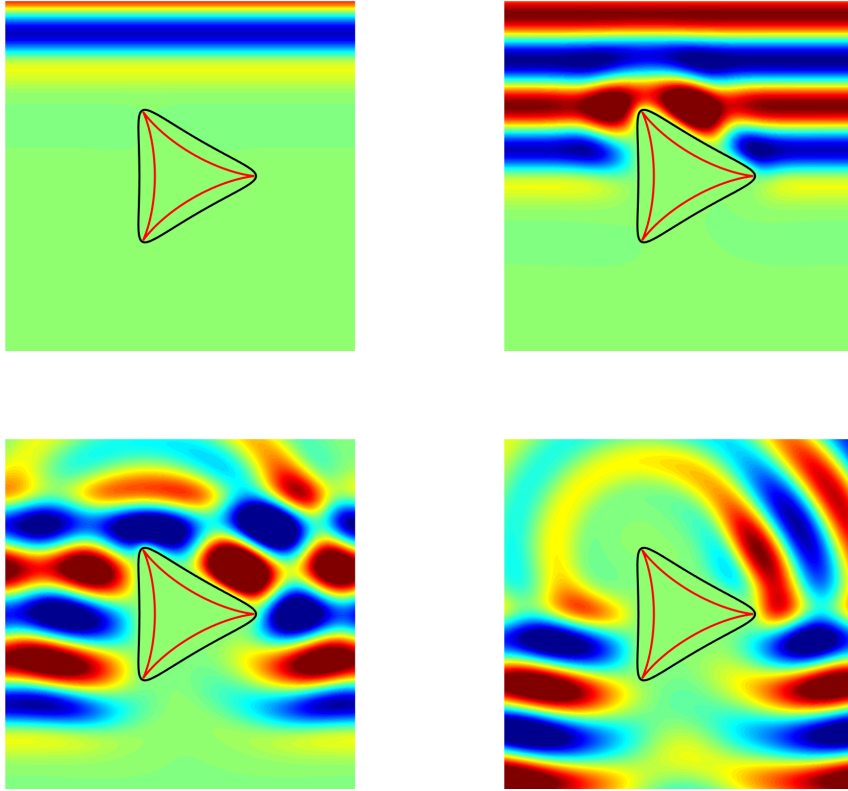
Fig. 8: Snapshots of the solution to the exterior problem in $[-3, 3] \times [-3, 3]$ at times $t = 2, 4, 6$ and 8.

tensions include a more elaborated method for the matrix compression consisting in Directional $\mathcal{H}^2-$matrices [6]. It is also possible to employ different MFS resolutions depending on the values of ζ_n. Adaptivity in terms of the real and imaginary parts of the wavenumber based on the residual of the least squares system could be incorporated.
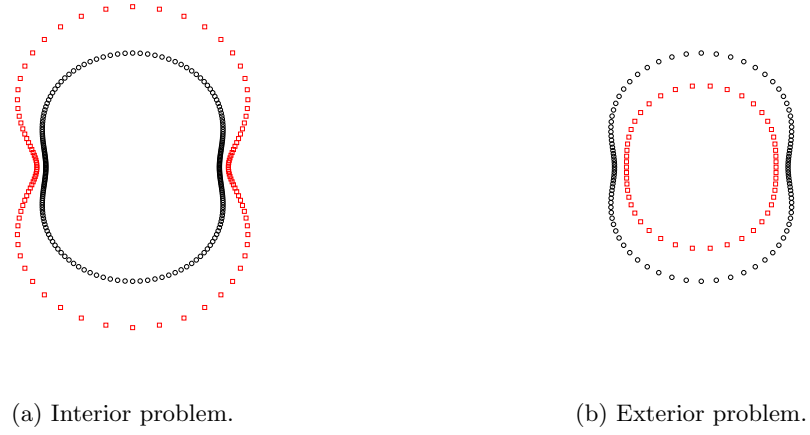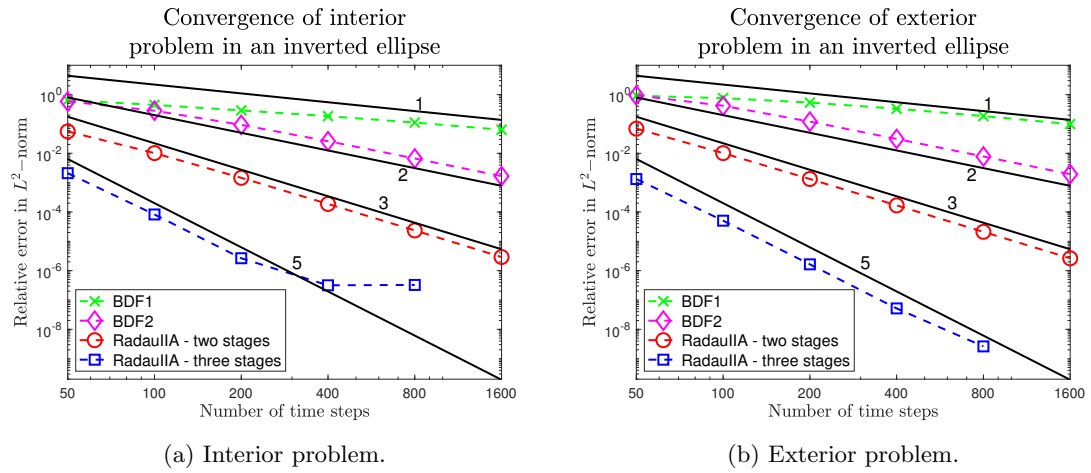
(a) Interior problem.   (b) Exterior problem.

Fig. 9: Inverted ellipse. Collocation points are marked as black circles, while source points are marked as red squares. Interior and exterior problem, respectively

(a) Interior problem.   (b) Exterior problem.

Fig. 10: Convergence of the CQ scheme for the interior/exterior problem in Section 4.4, compared with an (a) exact solution; (b) highly resolved solution.
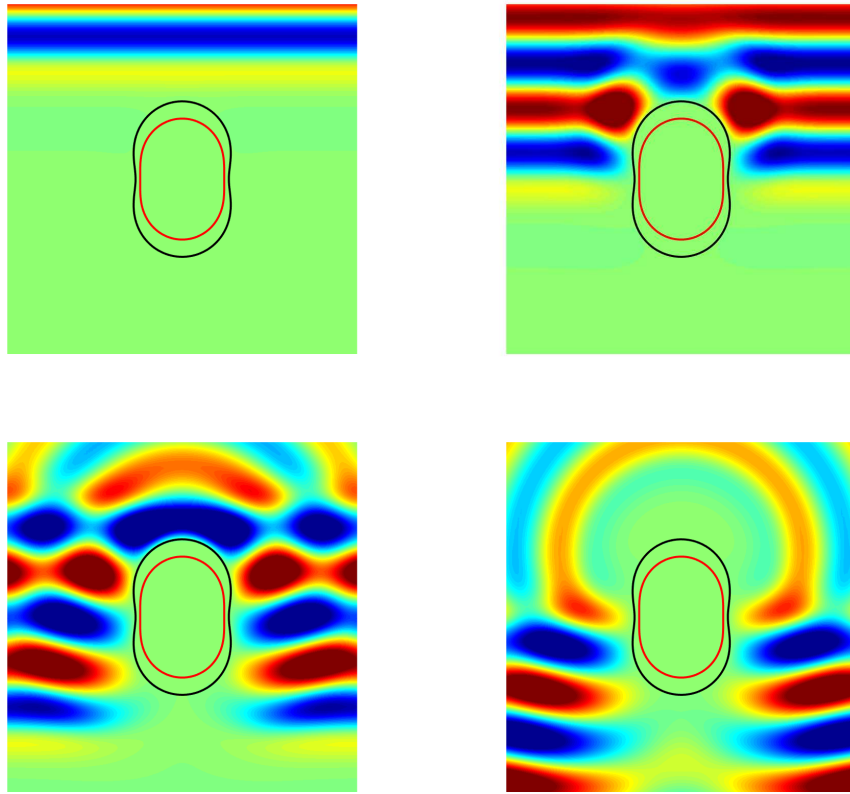
Fig. 11: Snapshots of the solution to the exterior problem in $[-3,3] \times [-3,3]$ at times $t = 2, 4, 6$ and 8.
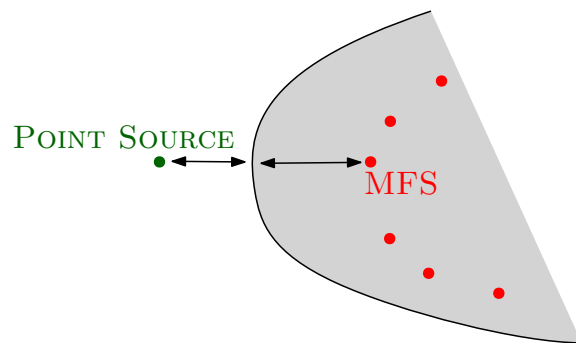

Fig. 12: Point source incident field too close to the scatterer in comparison with the sources associated to the MFS.
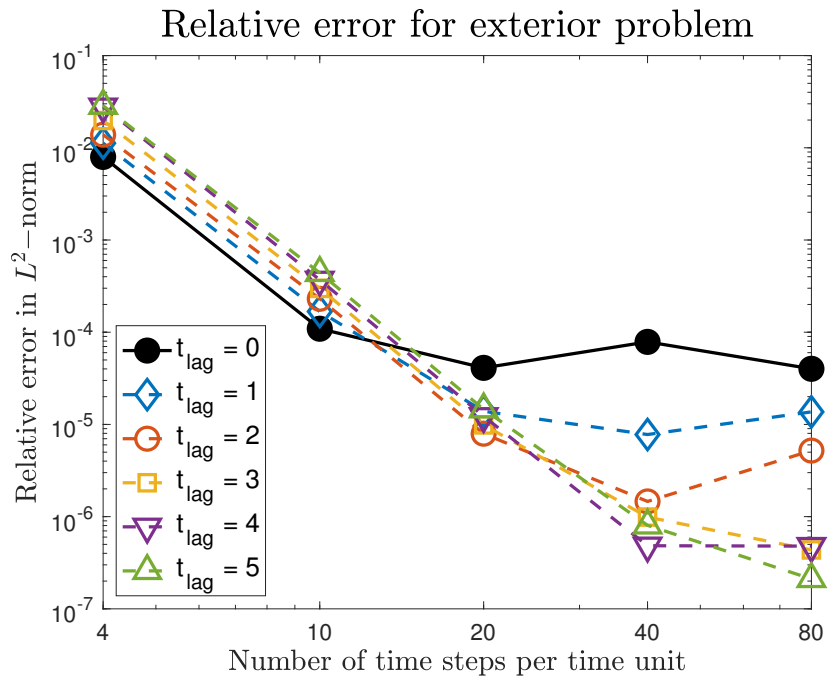
Fig. 13: Convergence of the CQ scheme with three stages RadauIIA method for the exterior problem in Section 4.5 for different time delays, compared with exact solutions.

Appendix. Source code for the numerical implementation of CQ and MFS can be found in https://github.com/ijlabarca/CQ-MFS. Tests and figures can be reproduced.

REFERENCES

[1] A. Aimi, M. Diligenti, C. Guardasoni, I. Mazzieri, and S. Panizzi, *An energy approach to space–time Galerkin BEM for wave propagation problems*, International journal for numerical methods in engineering, 80 (2009), pp. 1196–1240.

[2] L. Banjai, C. Lubich, and J. M. Melenk, *Runge–Kutta Convolution Quadrature for operators arising in Wave propagation*, Numerische Mathematik, 119 (2011), pp. 1–20.

[3] L. Banjai and S. Sauter, *Rapid Solution of the Wave Equation in Unbounded Domains*, SIAM Journal on Numerical Analysis, 47 (2008), pp. 227–249.

[4] A. H. Barnett and T. Betcke, *Stability and convergence of the Method of Fundamental Solutions for Helmholtz problems on analytic domains*, Journal of Computational Physics, 227 (2008), pp. 7003–7026.

[5] T. Betcke, N. Salles, and W. Smigaj, *Overresolving in the Laplace Domain for Convolution Quadrature methods*, SIAM Journal on Scientific Computing, 39 (2017), pp. A188–A213.

[6] S. Börm, M. Lopez-Fernandez, and S. Sauter, *Variable Order, Directional H2-Matrices for Helmholtz Problems with Complex Frequency*, arXiv preprint arXiv:1903.02803, (2019).

[7] C. Chen, X. Jiang, W. Chen, and G. Yao, *Fast Solution for Solving the Modified Helmholtz Equation with the Method of Fundamental Solutions*, Communications in Computational Physics, 17 (2015), pp. 867–886.

[8] P. J. Davies and D. B. Duncan, *Stability and convergence of collocation schemes for retarded potential integral equations*, SIAM Journal on Numerical Analysis, 42 (2004), pp. 1167–1188.

[9] A. B. et T. Ha Duong and J. Nedelec, *Formulation variationnelle espace-temps pour le calcul par potentiel retardé de la diffraction d'une onde acoustique (i)*, Mathematical methods in the applied sciences, 8 (1986), pp. 405–435.

[10] G. Fairweather and A. Karageorghis, *The method of fundamental solutions for elliptic boundary value problems*, Advances in Computational Mathematics, 9 (1998), p. 69.

[11] T. Ha-Duong, *On retarded potential boundary integral equations and their discretisation*, in Topics in computational wave propagation, Springer, 2003, pp. 301–336.

[12] C. Hafner, *The Generalized Multipole technique for Computational Electromagnetics*, Artech House Boston, 1990.

[13] C. Hafner and L. Bomholt, *The 3D Electrodynamic Wave Simulator-3D MMP Software and Users Guide*, 1995.

[14] M. Hassell and F.-J. Sayas, *Convolution Quadrature for Wave simulations*, in Numerical simulation in physics and engineering, Springer, 2016, pp. 71–159.

[15] M. Katsurada and H. Okamoto, *The collocation points of the fundamental solution method for the potential problem*, Computers & Mathematics with Applications, 31 (1996), pp. 123–137.

[16] J. Lin, C. Chen, and C.-S. Liu, *Fast solution of three-dimensional Modified Helmholtz equations by the Method of Fundamental Solutions*, Communications in Computational Physics, 20 (2016), pp. 512–533.

[17] C. Lubich, *Convolution Quadrature and Discretized Operational Calculus. I*, Numerische Mathematik, 52 (1988), pp. 129–145.

[18] C. Lubich, *Convolution Quadrature and Discretized Operational Calculus. II*, Numerische Mathematik, 52 (1988), pp. 413–425.

[19] C. Lubich and A. Ostermann, *Runge-Kutta Methods for Parabolic Equations and Convolution Quadrature*, Mathematics of Computation, 60 (1993), pp. 105–131.

[20] F.-J. Sayas, *Retarded Potentials and Time Domain Boundary Integral Equations: A Road Map*, vol. 50, Springer, 2016.

[21] G. Wanner and E. Hairer, *Solving ordinary differential equations II*, Springer Berlin Heidelberg, 1996.

[22] G. Wanner, E. Hairer, and S. P. Norsett, *Solving ordinary differential equations I*, Springer Berlin Heidelberg, 1993.